Potential flow inside an evaporating cylindrical line

A. J. Petsi[1,2] and V. N. Burganos[1,*]
[1]*Institute of Chemical Engineering and High Temperature Chemical Processes, Foundation for Research and Technology, Hellas, Greece*
[2]*Department of Chemical Engineering, University of Patras, 26504, Patras, Greece*
(Received 19 April 2005; published 28 October 2005)

An analytical solution to the problem of potential flow inside an evaporating line is obtained. The line is shaped as a half-cylinder lying on a substrate, and evaporates with either pinned or depinned contact lines. The solution is provided through the technique of separation of variables in the velocity potential and stream function formulations. Based on the flow field calculations, it is estimated that the coffee-stain phenomenon should be expected even for uniform evaporation flux throughout the cylindrical surface, provided that the contact lines remain anchored. A simple expression for the velocity potential is also suggested, which reproduces the local velocity vector with excellent accuracy. The vertically averaged velocity is calculated also for other contact line values, revealing for any value an outward liquid flow for pinned lines as opposed to inward flow for depinned lines.

DOI: 10.1103/PhysRevE.72.047301 PACS number(s): 47.55.Dz

I. INTRODUCTION

The evaporation of liquid segments with cylindrical geometry is encountered in a number of practical applications, including graphic-art drawing and printing, product marking and coding, substrate patterning in microelectronics, etc. Recently, there has been increasing interest in the fabrication of high-resolution thin-film transistors, which requires the controlled deposition of source, drain, and gate electrodes with tailored dimensions, within conveniently selected microchannels [1,2]. A key stage in this type of fabrication process is the evaporation of the solvent following the touch-down, spreading, and equilibration of the droplet that is ejected from an ink-jet orifice. It has been observed experimentally that the characteristic time of the spreading stage is usually much shorter than that of the evaporation stage, depending of course on the nature of the solvent and on the size of the droplet. For modeling purposes, this observation allows the separate study of the evaporation process from that of spreading, and justifies the usual assumption of a static droplet, shaped as a spherical or cylindrical cap prior to the initiation of the evaporation [3], due mainly to the action of the surface tension.

Several attempts to describe the internal flow during droplet evaporation have been reported in the literature and can be, in general, divided in two main categories. In the first one, the flow field in the interior of the droplet is determined through rigorous or approximate analytical solutions, whereas in the second, only the vertically averaged liquid velocity is calculated, which nevertheless provides a useful picture of the mean microflow. In the former case, an analytical solution was recently provided in [4], assuming a hemispherical droplet, potential flow conditions inside the droplet, and diffusion-controlled evaporation. Thanks to the use of a contact angle equal to $\pi/2$, the evaporation flux is uniform on the surface of the droplet in both the diffusion and the kinetic regimes. The results for the local velocity field inside the droplet contribute significantly to our understanding of the so-called coffee-stain effect and can be further used to calculate the deposition of colloidal particles suspended in the droplet, which eventually make up the solid electrode. Lubrication solutions for the flow field are possible [5,6], but their validity is limited to thin droplets only. In the second case, the vertically averaged velocity is calculated from a mass balance [3] without any detailed information on the local flow field. Nevertheless, the trend of the colloidal particle rearrangement within the liquid phase can thus be delineated and studied in terms of the evaporation mechanism and the mobility of the contact lines.

In the present work, the liquid is arranged as a half-cylinder lying on a flat substrate with a contact angle $\theta_c = \pi/2$. Evaporation takes place from the surface of the cylinder at uniform flux, which is consistent with both kinetically controlled and diffusion-controlled evaporation processes for the particular contact angle. The length of the cylinder is much larger than the diameter, which justifies the use of the term *liquid line* in the rest of the paper. Potential flow is assumed within the liquid mass under the pinning assumption, which has been repeatedly verified experimentally for various colloidal suspensions, at least at the initial stages of the evaporation process. The constant contact angle mode, combined with moving contact lines, has also been observed experimentally, most notably during evaporation of pure solvents (see, for instance, relevant sections in [3,7–10]). Analytical solutions are obtained here for the stream function and the velocity potential in the pinned line case, whereas the trivial solution applies in the depinned case. Finally, analytical expressions for the vertically averaged velocity are provided for both the pinned and depinned line cases, which are valid for any value of the contact angle in $(0, \pi/2)$.

II. MODEL DEVELOPMENT AND SOLUTION

Consider a liquid line shaped as a half-cylinder of infinite length lying on a flat surface. Gravity effects can be safely

*Corresponding author; electronic address: vbur@iceht.forth.gr

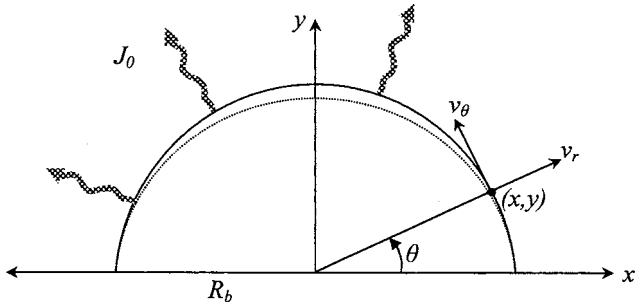

FIG. 1. Schematic representation of evaporating line and coordinate system.

neglected for small droplets (<1 mm), for which the Bond number is considerably less than 1 [4]. Surface evaporation is assumed to take place through a uniform evaporation flux from the cylindrical surface. Such an assumption is valid in both the kinetic and the diffusion regime for $\theta_c=\pi/2$. If the contact lines are pinned, then considerable liquid flow is expected to take place inside the line in order to provide the necessary flow towards the contact lines and to replenish the mass that is evaporated there. In this way, the line edges remain wet, as required by the line-anchoring condition.

In typical printing applications, the length of the liquid lines is much larger than their width and, hence, the problem can be solved on a cross section only using polar coordinates. For potential flow at steady state, we can write

$$\frac{1}{r}\frac{\partial}{\partial r}\left(r\frac{\partial\varphi}{\partial r}\right)+\frac{1}{r^2}\frac{\partial^2\varphi}{\partial\theta^2}=0, \tag{1}$$

where φ is the velocity potential, which is connected to the radial and angular velocity components (see Fig. 1) through the relations $v_r=\partial\varphi/\partial r$ and $v_\theta=(1/r)(\partial\varphi/\partial\theta)$. Equation (1) must be solved for φ subject to the following boundary conditions:

axial symmetry

$$\frac{\partial\varphi}{\partial\theta}=0, \quad \text{at } \theta=\frac{\pi}{2}, \tag{2a}$$

no flow through the solid surface

$$\frac{\partial\varphi}{\partial\theta}=0, \quad \text{at } \theta=0, \tag{2b}$$

finite solution at the center

$$\varphi=finite, \quad \text{at } r=0, \tag{2c}$$

radial liquid velocity at the surface

$$\frac{\partial\varphi}{\partial r}=u_{rs}+\frac{J_0}{\rho}, \tag{2d}$$

given in terms of the evaporation flux J_0 and of the radial component of the surface velocity u_{rs}, where ρ is the liquid density.

If θ_c is the contact angle and R_b the half-width of the wetted area, the volume of the liquid per unit length is

$$V_L=R_b^2\frac{\theta_c-\cos\theta_c\sin\theta_c}{\sin^2\theta_c}. \tag{3}$$

The total evaporation rate per unit length is given by

$$-\rho\frac{dV_L}{dt}=2J_0\frac{\theta_c}{\sin\theta_c}R_b. \tag{4}$$

If h_0 stands for the height of the liquid at the center, then

$$h_0=R_b\frac{1-\cos\theta_c}{\sin\theta_c}, \tag{5}$$

and

$$\frac{dh_0}{dt}=-\frac{J_0}{\rho}\frac{\theta_c(1-\cos\theta_c)}{\sin\theta_c-\theta_c\cos\theta_c} \tag{6}$$

for pinned contact lines.

The radial component of the interface velocity is given by

$$u_{rs}=\frac{(\partial h/\partial t)_x}{\left[1+\left(\frac{\partial h}{\partial x}\right)_t^2\right]^{1/2}}, \tag{7}$$

where h is the height at position x.

However,

$$h=(R^2-x^2)^{1/2}-(R-h_0), \tag{8}$$

where R is the cylinder radius. Following algebraic manipulations, we finally get

$$\left(\frac{\partial h}{\partial t}\right)_x=\frac{dh_0}{dt}, \quad \text{for } \theta_c=\pi/2 \tag{9}$$

and

$$\left(\frac{\partial h}{\partial x}\right)_t=-\frac{x}{(R^2-x^2)^{1/2}}, \quad \text{for any } \theta_c \text{ value}. \tag{10}$$

Introduction of expressions (6), (9), and (10) into Eq. (7) gives

$$u_{rs}=-\frac{J_0}{\rho}\frac{\pi}{2}\sin\theta. \tag{11}$$

Use of expression (11) in Eq. (2d) yields

$$\frac{\partial\varphi}{\partial r}=\frac{J_0}{\rho}\left(1-\frac{\pi}{2}\sin\theta\right). \tag{12}$$

The solution to Eq. (1) subject to conditions (2a) and (2b) is

$$\varphi(r,\theta)=A_0+B_0\ln r+\sum_{n=1}^{\infty}(A_n r^{2n}+B_n r^{-2n})\cos 2n\theta,$$

which reduces to

$$\varphi(r,\theta)=A_0+\sum_{n=1}^{\infty}A_n r^{2n}\cos 2n\theta \tag{13}$$

upon use of condition (2c). The unknown coefficients $A_n, n=1,2,\ldots$ can be obtained with the help of Eq. (2d), written in the form of Eq. (12), and are given by

$$A_n = \frac{J_0}{\rho}\frac{R^{-2n+1}}{n(4n^2-1)}, \quad n = 1,2,\ldots .$$

The final expression for the velocity potential, within an arbitrary constant, is

$$\varphi(r,\theta) = \frac{J_0 R}{\rho}\sum_{n=1}^{\infty}\frac{(r/R)^{2n}\cos 2n\theta}{n(4n^2-1)}. \tag{14}$$

Obviously, once the general solution of Eq. (13) is available, other types of evaporation mechanisms with $J_0=J(\theta)$ can also be handled. The radial and angular components of the velocity vector can be calculated at every point from

$$v_r = \frac{2J_0}{\rho}\sum_{n=1}^{\infty}\frac{(r/R)^{2n-1}\cos 2n\theta}{4n^2-1} \tag{15a}$$

and

$$v_\theta = -\frac{2J_0}{\rho}\sum_{n=1}^{\infty}\frac{(r/R)^{2n-1}\sin 2n\theta}{4n^2-1}. \tag{15b}$$

In the stream function formulation,

$$\Delta\psi = 0. \tag{16}$$

Using the same set of boundary conditions as above, adjusted to the ψ-formulation, and using the technique of separation of variables, one eventually gets

$$\psi = \frac{J_0 R}{\rho}\sum_{n=1}^{\infty}\frac{(r/R)^{2n}\sin 2n\theta}{n(4n^2-1)}.$$

This expression reproduces, of course, the same expressions for v_r and v_θ (15a) and (15b) as those obtained in the velocity potential formulation.

III. RESULTS AND DISCUSSION

The flow field in terms of the local velocity vector is shown in Fig. 2. Note that the internal flow is directed from the center to the edges of the line, thus promoting a ring-like deposit for colloidal dispersions. This flow configuration develops despite the evaporation flux uniformity on the liquid surface and is caused by the line anchoring condition. Notice that the liquid velocity is proportional to the magnitude of the local evaporation flux (J_0), which implies that the coffee-stain phenomenon becomes more pronounced with increasing volatility of the solvent. The sign of the radial velocity changes at $\theta=\sin^{-1}(2/\pi)\approx 2\pi/9$, whereas the corresponding angle in the spherical geometry is $\pi/6$, based on the work in [4]. Needless to say, the full description of the problem dynamics requires the solution of the same problem at an arbitrary contact angle followed by monitoring particle trajectories in the interior of the evaporating line to their eventual deposit on the surface.

It is noteworthy that the first few terms of the solution expansion shown in Eq. (14) provide a very good approximation to the full solution for practically any position inside the line. In fact, numerical calculations reveal that the simple expression (truncation at $n=2$)

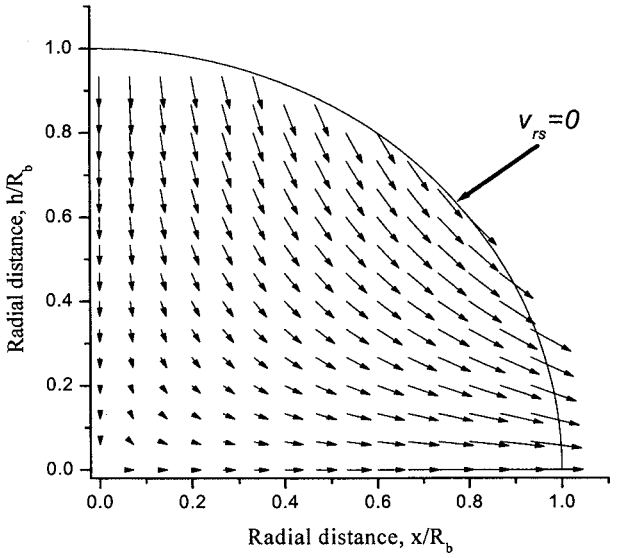

FIG. 2. Vector representation of the internal flow field in an evaporating cylindrical line.

$$\varphi(r,\theta) \approx \frac{J_0 R}{\rho}\left(\frac{r^2\cos 2\theta}{3R^2} + \frac{r^4\cos 4\theta}{30R^4}\right) \tag{17}$$

reproduces the actual velocity with 99% accuracy, except at positions very close to the surface, where a few more terms are needed to achieve the same level of accuracy (see Fig. 3). This facilitates considerably the flow field calculations in the vast majority of the liquid volume.

In the case of pure solvents, it is reasonable to expect that θ_c remains constant during evaporation and the contact lines are allowed to slip on the surface. In this case, the interface velocity is everywhere the same and equal to dR/dt. But a simple mass balance at the surface yields $dR/dt=-J_0/\rho$. Consequently, the radial component of the liquid velocity vanishes at the surface and Eqs. (1) and (16) have only the

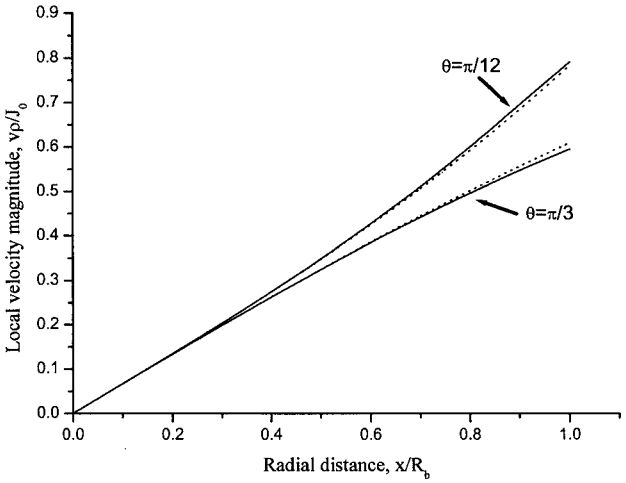

FIG. 3. Comparison of the use of the full (solid lines) and approximate (dashed lines) solution, as given by Eqs. (14) and (17), respectively, for the calculation of the dimensionless local velocity magnitude at two different angular positions.

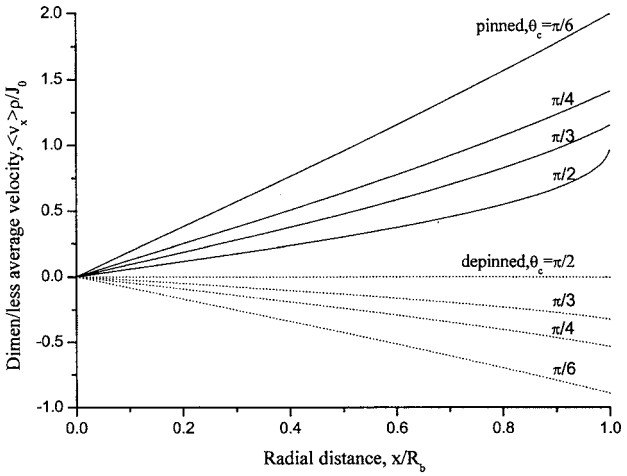

FIG. 4. Dimensionless vertically averaged velocity vs dimensionless radial distance on the substrate for pinned (solid curves) and depinned (dotted curves) contact lines. Variation with the contact angle value.

trivial solution (no flow inside the liquid mass). However, this is only the case of uniform evaporation flux on the surface with depinned contact lines. Under different conditions, including those related to stronger or weaker wettabilities than the one considered here, finite flow is expected to develop inside the liquid line.

A practical quantity that provides a good measure of the inward or outward flow trend is the vertically averaged liquid velocity. It can be calculated from

$$\langle v_x \rangle = \frac{1}{h}\int_0^h v_x dy, \tag{18}$$

where $v_x = v_r \cos\theta - v_\theta \sin\theta$ is the x-component of the liquid velocity in the Cartesian coordinate system. Alternatively, one can calculate this velocity directly from the mass balance around a vertical liquid column of width δx and height h (see [3,11] for a similar analysis in spherical droplets)

$$\rho\left(\frac{\partial h}{\partial t}\right)_x = -\rho\left(\frac{\partial \langle v_x\rangle h}{\partial x}\right)_t - J_0\left[1+\left(\frac{\partial h}{\partial x}\right)^2\right]^{1/2},$$

which yields

$$\langle v_x\rangle = -\frac{1}{\rho h}\int_0^x \left\{\rho\left(\frac{\partial h}{\partial t}\right)_x + J_0\left[1+\left(\frac{\partial h}{\partial x}\right)^2\right]^{1/2}\right\} dx. \tag{19}$$

Introduction of Eqs. (9) and (10) into Eq. (19) leads eventually to

$$\langle v_x\rangle = \frac{J_0}{\rho}\frac{\frac{\pi}{2}\bar{x} - \sin^{-1}(\bar{x})}{[1-\bar{x}^2]^{1/2}}, \tag{20}$$

where $\bar{x} = x/R_b$. In the general case of $\theta_c \neq \pi/2$, one can show following algebraic manipulations that

$$\langle v_x\rangle = \frac{J_0}{\rho \bar{h}}\frac{1}{(\theta_c \cos\theta_c - \sin\theta_c)}[\sin^{-1}(\bar{x}\sin\theta_c) - \bar{x}\theta_c],$$

and

$$\langle v_x\rangle = \frac{J_0}{\rho \bar{h}}\frac{\cos\theta_c}{(\theta_c - \sin\theta_c\cos\theta_c)}[\sin^{-1}(\bar{x}\sin\theta_c) - \bar{x}\theta_c],$$

in the pinned and depinned line cases, respectively, where $\bar{h} = h/R_b$. Figure 4 shows the variation of the vertically averaged liquid velocity with the dimensionless distance from the center for various values of the contact angle and for both types of contact line conditions. Outward flow is obtained for any contact angle value in the pinned line case, whereas inward flow is obtained in the depinned line case. This is a very interesting result as it reveals that, under potential flow conditions, the coffee-stain effect is always to be expected for intermediate and low wettability substrates, provided that the contact lines remain pinned. On the contrary, concentration of the deposit around the line center is expected for moving contact lines, for low and intermediate substrate wettability.

[1] H. Sirringhaus, T. Kawase, R. H. Friend, T. Shimoda, M. Inbasekaran, W. Wu, and E. P. Woo, Science **290**, 2123 (2000).
[2] T. Kawase, T. Shimoda, C. Newsome, H. Sirringhaus, and R. H. Friend, Thin Solid Films **438–439**, 279 (2003).
[3] R. D. Deegan, O. Bakajin, T. F. Dupont, G. Huber, S. R. Nagel, and T. A. Witten, Phys. Rev. E **62**, 756 (2000).
[4] Y. Y. Tarasevich, Phys. Rev. E **71**, 027301 (2005).
[5] M. Chopra, L. Li, H. Hu, M. A. Burns, and R. G. Larson, J. Rheol. **47**, 1111 (2003).
[6] B. J. Fischer, Langmuir **18**, 60 (2002).
[7] C. Bourgès-Monnier and M. E. R. Shanahan, Langmuir **11**, 2820 (1995).
[8] R. D. Deegan, O. Bakajin, T. F. Dupont, G. Huber, S. R. Nagel, and T. A. Witten, Nature (London) **389**, 827 (1997).
[9] M. Cachile, O. Bénichou, and A. M. Cazabat, Langmuir **18**, 7985 (2002).
[10] H. Hu and R. G. Larson, J. Phys. Chem. B **106**, 1334 (2002).
[11] Y. O. Popov and T. A. Witten, Phys. Rev. E **68**, 036306 (2003).